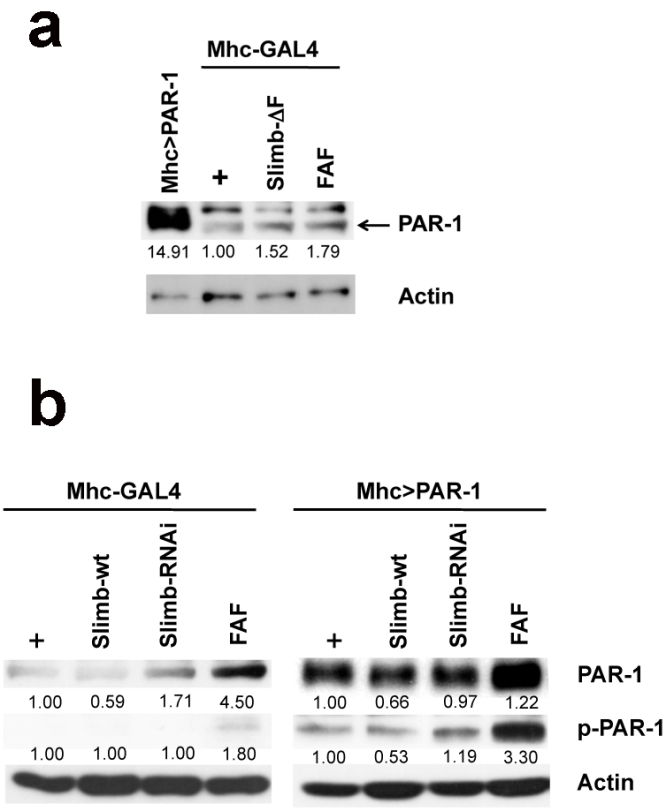

Supplementary Figure S1. Western blot analysis of PAR-1 and p-PAR-1 levels in various genotypes. (a) Western blot analysis comparing levels of endogenous PAR-1 after Slimb or FAF manipulation using the muscle-specific *Mhc-Gal4* driver that did not affect NMJ bouton number, with the level of transgenic PAR-1 in *Mhc-Gal4>PAR-1* animals that showed reduced bouton number. **(b)** Western blot analysis of endogenous PAR-1 and p-PAR-1 protein levels or transgenic PAR-1 and p-PAR-1 levels after Slimb or FAF manipulation. *Mhc-Gal4* was used to direct transgene expression. Actin serves as a loading control. Values represent normalized PAR-1 or p-PAR-1 levels from three independent experiments.

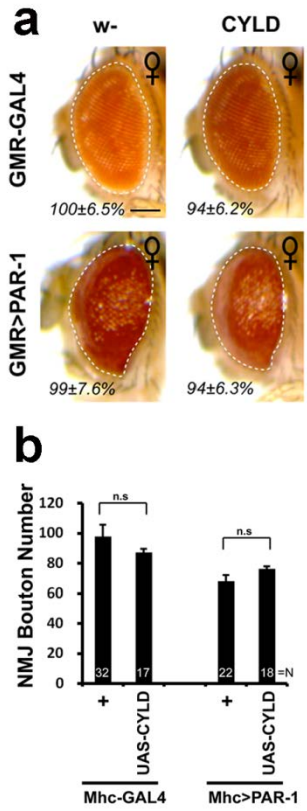

Supplementary Figure S2. Genetic interaction tests between PAR-1 and CYLD in the fly eye and NMJ. (a) Testing for genetic interaction between PAR-1 and CYLD in the fly eye. All flies were raised at 25^{o}C. Images of female flies are shown. CYLD failed to modify PAR-1 induced rough eye phenotype. The genotypes are: *GMR-Gal4/+* (n=16), *GMR-Gal4>UAS-CYLD* (n=16), *GMR-Gal4>UAS-PAR-1* (n=17) and *GMR-Gal4>UAS-PAR-1+UAS-CYLD* (n=17). Experiments were performed in triplicate. Dashed lines outline the eye contour. Values represent areas of retinal surface normalized with *GMR-Gal4/+* control. Scale bar: 100 μm. **(b)** Testing for genetic interaction between PAR-1 and CYLD in the NMJ. The bar graph shows quantification of bouton numbers in the indicated genotypes. Postsynaptic co-expression of CYLD did not affect the bouton loss phenotype caused by PAR-1 overexpression. N indicates the number of animals analyzed. The error bars represent means ± SEM. *P*-values were determined using two-tailed Student's *t*-test for each comparison. Experiments were performed in triplicate.

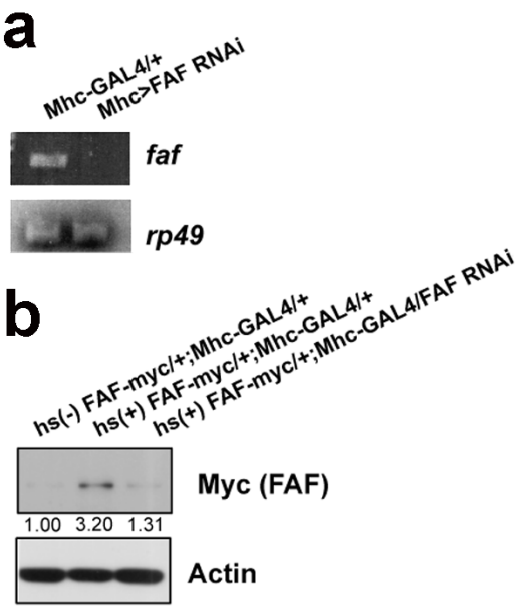

Supplementary Figure S3. Validating the efficiency of the FAF RNAi transgene used in this study. (a) RT-PCR analysis of *FAF* mRNA levels in wild-type and *Mhc-Gal4>FAF RNAi* larvae. Total RNAs prepared from third instar larval body wall muscle were used. *Rp49* serves as a loading control. **(b)** Western blot analysis showing that the FAF RNAi transgene efficiently knocked down the expression of FAF-Myc protein expressed from an *hs-FAF-Myc* transgene. Thoracic extracts prepared from heat-shocked adult animals were used. Actin serves as a loading control. Values represent averaged FAF-Myc levels normalized with non heat-shock control, which shows basal leaky expression of the transgene, from three independent experiments.

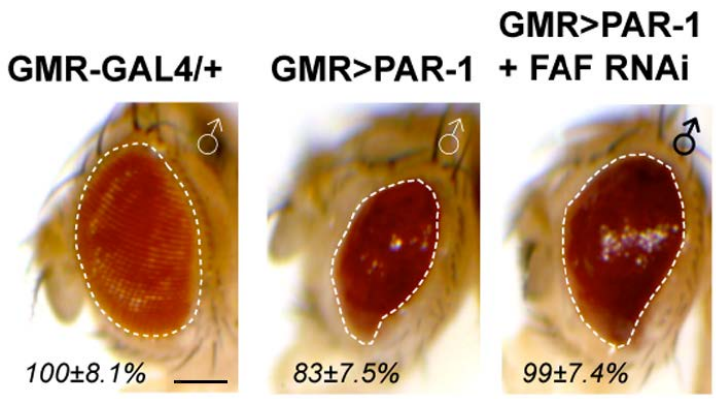

Supplementary Figure S4. Genetic interaction between PAR-1 and FAF in the fly eye. The reduced eye size caused by PAR-1 overexpression was rescued by FAF RNAi. Eye images of male flies of the indicated genotypes are shown. The genotypes are: *GMR-Gal4/+* (n=16), *GMR-Gal4>UAS-PAR-1* (n=18) and *GMR-Gal4>UAS-PAR-1+UAS-FAF RNAi* (n=17). Experiments were performed in triplicate. Dashed lines outline the eye contour. Values represent areas of retinal surface normalized with *GMR-Gal4/+* control. Scale bar: 100 μm.

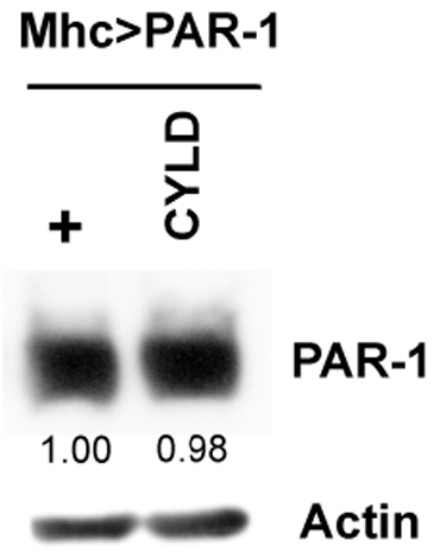

Supplementary Figure S5. Western blot analysis showing that a control deubiquitinating enzyme CYLD did not significantly affect PAR-1 protein level. Actin serves as a loading control. Values represent PAR-1 levels normalized by actin levels from three independent experiments.

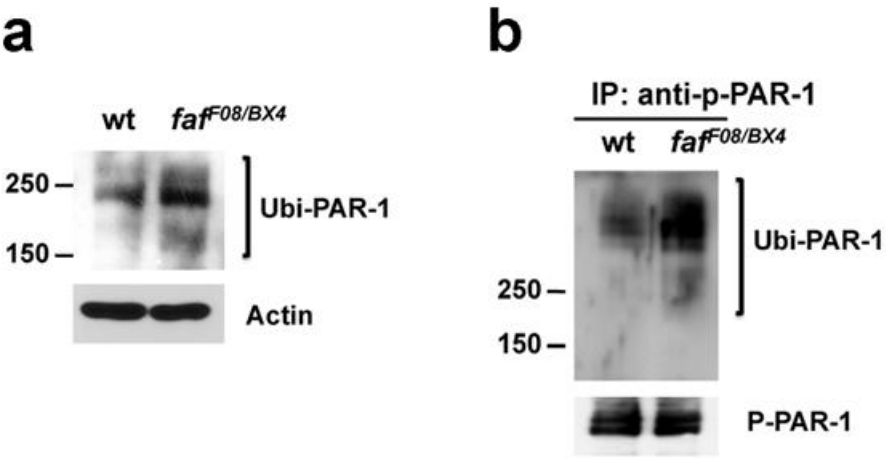

Supplementary Figure S6. Ubiquitinated forms of PAR-1 and p-PAR-1 accumulate in *faf* mutant. (a) Western blot analysis showing moderate increase of ubiquitinated forms of PAR-1 in faf^{F08}/faf^{BX4} mutant thorax extracts. Actin serves as a loading control. **(b)** Western blot analysis showing a dramatic increase of ubiquitination p-PAR-1 immunoprecipated from faf^{F08}/faf^{BX4} mutant fly head extracts. Brackets indicate ubiquitinated PAR-1 (Ub-PAR-1).

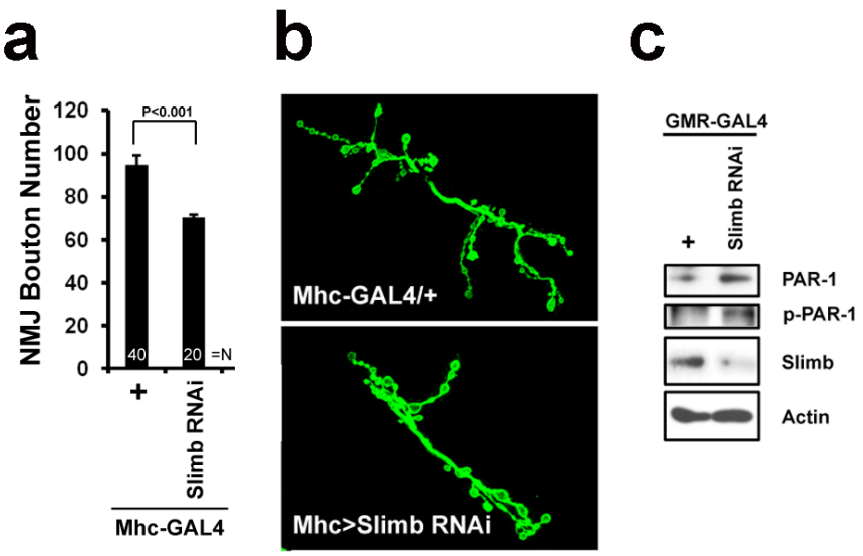

Supplementary Figure S7. Effects of inhibition of Slimb by RNAi on NMJ bouton number. (a) Quantification of data showing the effect of postsynaptic Slimb RNAi on the total number of boutons per muscle area on muscle 6/7 of A3. Significant difference in NMJ bouton number was observed in *Mhc-Gal4>UAS-Slimb RNAi* animals compared to *Mhc-Gal4*/+ control. N indicates the number of animals analyzed. N indicates the number of animals analyzed. The error bars represent means ± SEM. *P*-values were determined using two-tailed Student's *t*-test for each comparison. Experiments were performed in triplicate. (**b**) Representative immunostaining with anti-HRP showing NMJ morphology in the indicated genotypes. (**c**) Western blot analysis of endogenous PAR-1, p-PAR-1 and Slimb levels in *GMR>Slimb RNAi* animals. The Slimb RNAi transgene is effective in knocking down Slimb protein expression. Actin serves as a loading control.

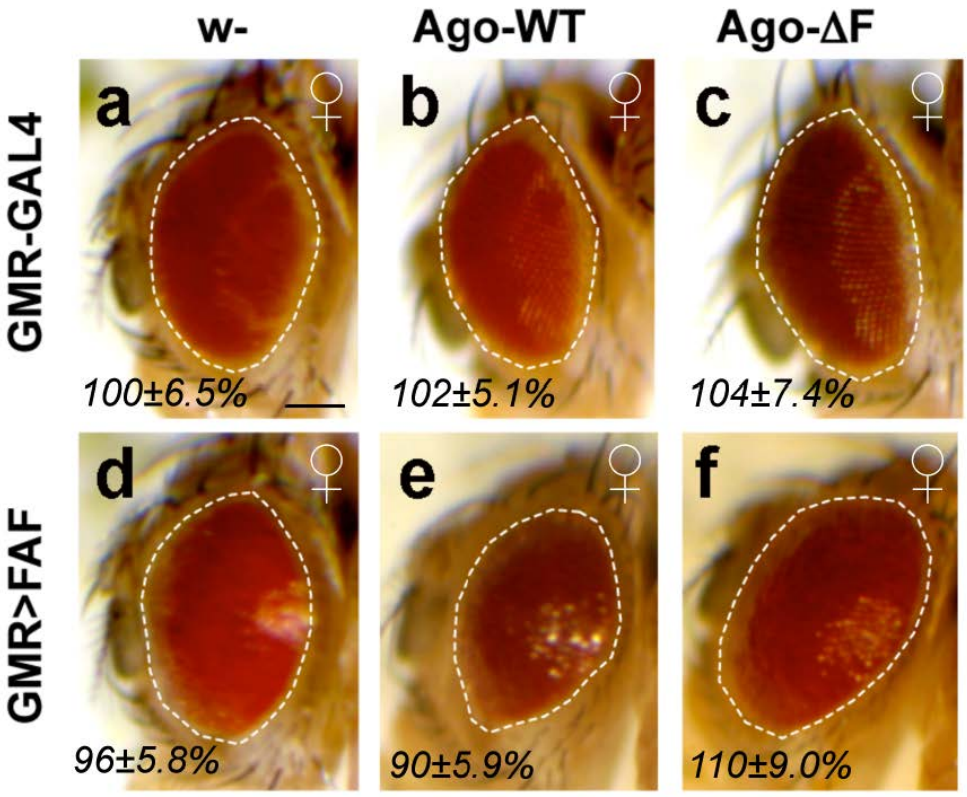

Supplementary Figure S8. Testing for genetic interaction between FAF and Ago in the fly Eye. Eye images of female flies of the indicated genotypes are shown. All flies were grown at 25^{o}C. There is no significant change of eye size or morphology in wild type or FAF(EP381) overexpression background with or without Ago transgene expression. The genotypes are: *GMR-Gal4/+* **(a)**, *GMR-Gal4>UAS-Ago-WT* **(b)**, *GMR-Gal4>UAS-Ago-ΔF* **(c)**, *GMR-Gal4>FAF^{EP381}* **(d)**, *GMR-Gal4>FAF^{EP381}+UAS-Ago-WT* **(e)**, and *GMR- Gal4>FAF^{EP381}+UAS-Ago-ΔF* **(f)** (n=16, 18, 17, 19, 16 and 16 animals, respectively). Experiments were performed in triplicate. Dashed lines outline the eye contour. Values represent areas of retinal surface normalized with *GMR-Gal4/+* control. Scale bar: 100 μm.

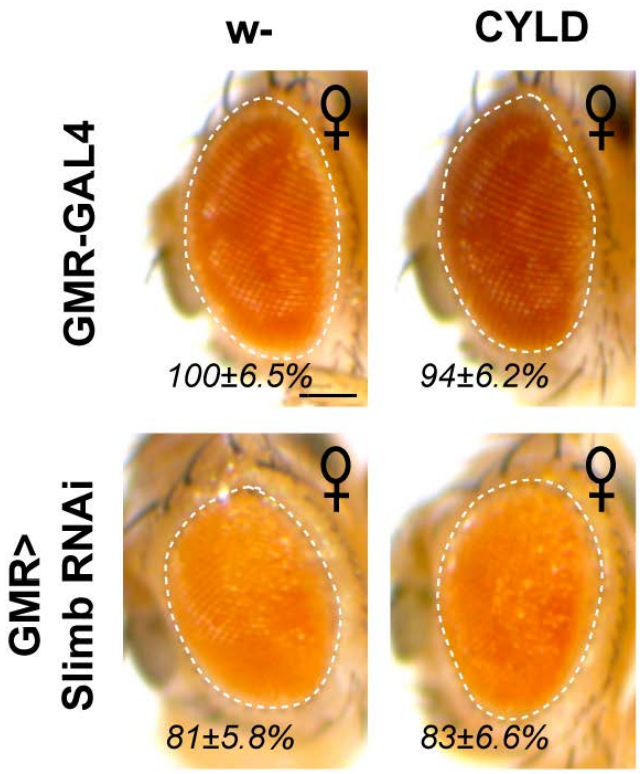

Supplementary Figure S9. Testing for genetic interaction between Slimb and CYLD in the fly eye. The genotypes are: *GMR-Gal4/+* (n=16), *GMR-Gal4>UAS-CYLD* (n=16), *GMR-Gal4>UAS-Slimb RNAi* (n=18) and *GMR-Gal4>UAS-Slimb RNAi+UAS-CYLD* (n=17). All flies were raised at 25^{o}C. Images of female flies are shown. No significant difference in eye size between *GMR>Slimb RNAi* and *GMR>Slimb RNAi+CYLD* was found. This result demonstrates that the genetic interaction between Slimb and FAF is specific. Experiments were performed in triplicate. Dashed lines outline the eye contour. Values represent areas of retinal surface normalized with *GMR-Gal4/+* control. Scale bar: 100 μm.

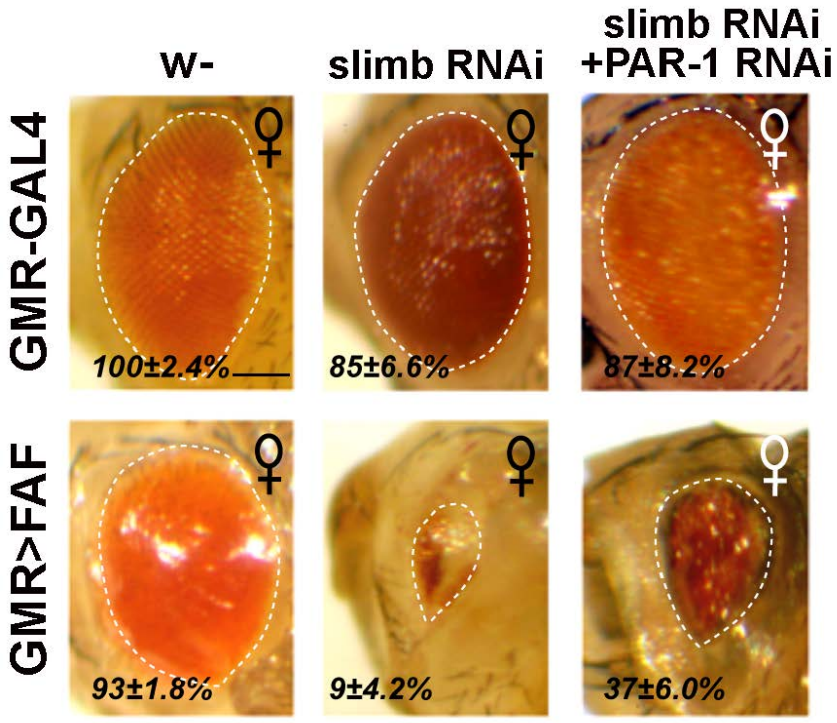

Supplementary Figure S10. Mediation of the genetic interaction between Slimb and FAF by PAR-1. The genotypes are: *GMR-Gal4/+* (n=10), *GMR-Gal4>UAS-Slimb RNAi* (n=11), *GMR-Gal4>UAS-Slimb RNAi+PAR-1 RNAi* (n=10), *GMR-Gal4>FAF*^{EP381} (n=10), *GMR-Gal4> FAF*^{EP381}*+UAS-Slimb RNAi* (n=9) and *GMR-Gal4> FAF*^{EP381}*+UAS-Slimb RNAi+PAR-1 RNAi* (n=10). Statistically significant differences are $P<0.001$ (*GMR-Gal4/+, GMR-Gal4>UAS-Slimb RNAi; GMR- Gal4>FAF*^{EP381}*, GMR-Gal4>FAF*^{EP381}*+UAS-Slimb RNAi; GMR- Gal4>FAF*^{EP381}*+UAS-Slimb RNAi, GMR-Gal4>FAF*^{EP381}*+UAS Slimb RNAi +UAS-PAR-1 RNAi*) as determined by Student's *t*-test. Experiments were performed in triplicate. All flies were raised at 22^{o}C. Because the co-expression of FAF and Slimb RNAi caused pupae lethality, images of pharate adult female flies dissected out of pupal cases are shown. The significant rescue of FAF and Slimb RNAi co-expression induced small eye phenotype by PAR-1 RNAi supports that the genetic interaction between Slimb and FAF is partially mediated by PAR-1. Other substrates likely contributes to the eye phenotype as well. Experiments were performed in triplicate. Dashed lines outline the eye contour. Values represent areas of retinal surface normalized with *GMR-Gal4/+* control. Scale bar: 100 μm.

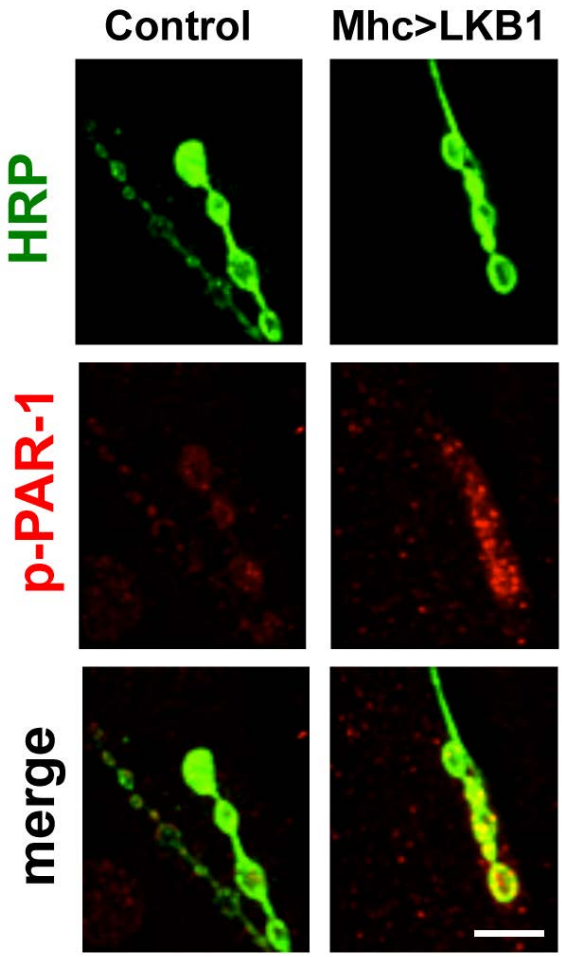

Supplementary Figure S11. Control experiment demonstrating the specificity of the phospho-PAR-1 signal detected in larval NMJ. Images show double labeling of larval NMJs with anti-HRP in green and anti-p-PAR-1 in red. p-PAR-1 signal is increased in LKB1 overexpression animals. Scale bars: 10 µm.

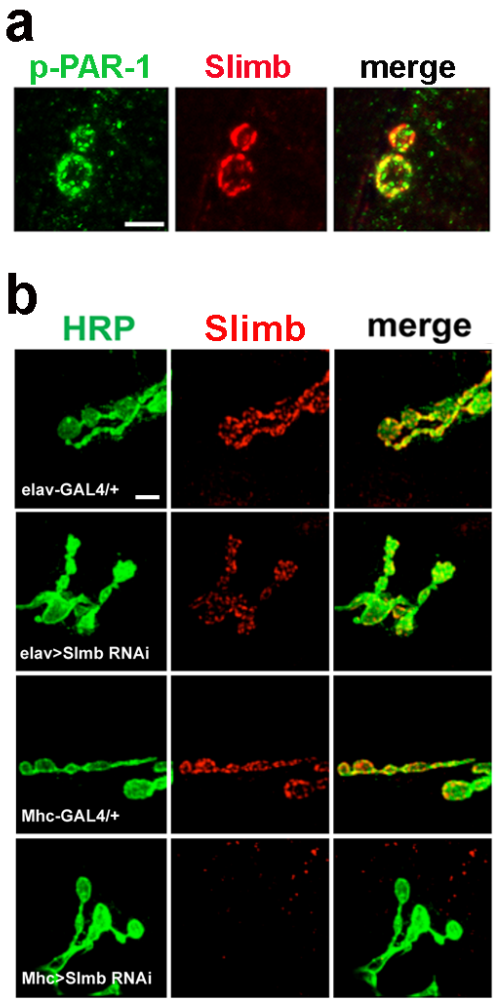

Supplementary Figure S12. Slimb expression is more enriched at the postsynaptic compartment. (a) Double-label experiment showing that phospho-PAR-1 (green) precisely co-localized with Slimb (red) at the larval NMJ. **(b)** Double-labeling with anti-HRP (green) and anti-Slimb (red) showing the effects of pre- (*elav-Gal4* driven) or post-synaptic (*Mhc-Gal4* driven) RNAi knockdown of Slimb on synaptic Slimb signals. Scale bars: a and b, 5 µm.

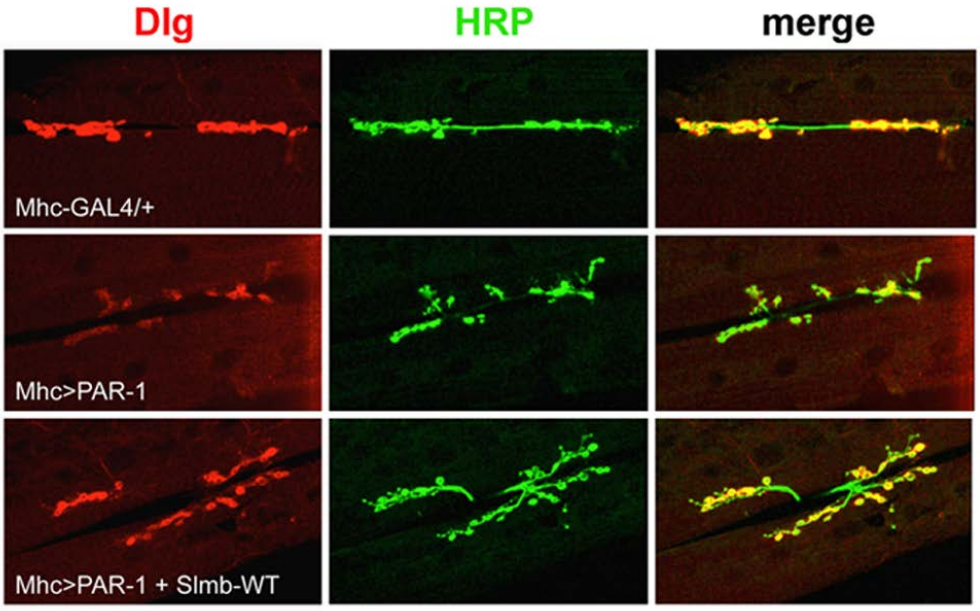

Supplementary Figure S13. Rescue of PAR-1 overexpression induced Dlg mislocalization by Slimb. Co-expression of Slimb-WT largely rescued the Dlg delocalization phenotype caused by PAR-1 overexpression. Double-labeling of larval NMJs of the indicated genotypes with anti-Dlg (red), anti-HRP (green), and merged images are shown.

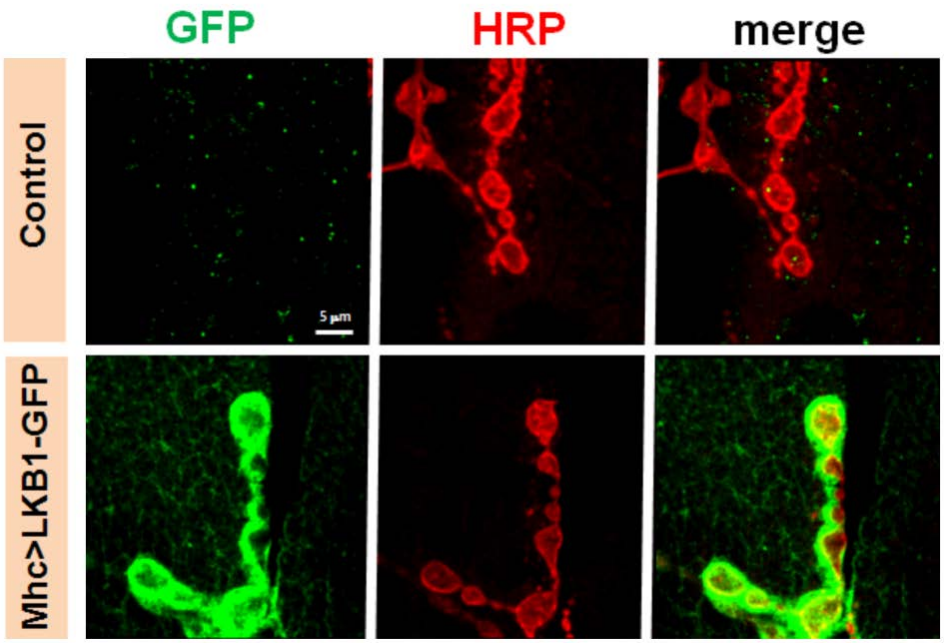

Supplementary Figure S14. Localization of LKB1-GFP at the larval NMJ. Double-labeling with anti-HRP (red) and anti-GFP (green) of wild-type, *elav-Gal4>LKB1-GFP*, or *Mhc-Gal4>LKB1-GFP* larval NMJs are shown. Scale bars: 5 μm.

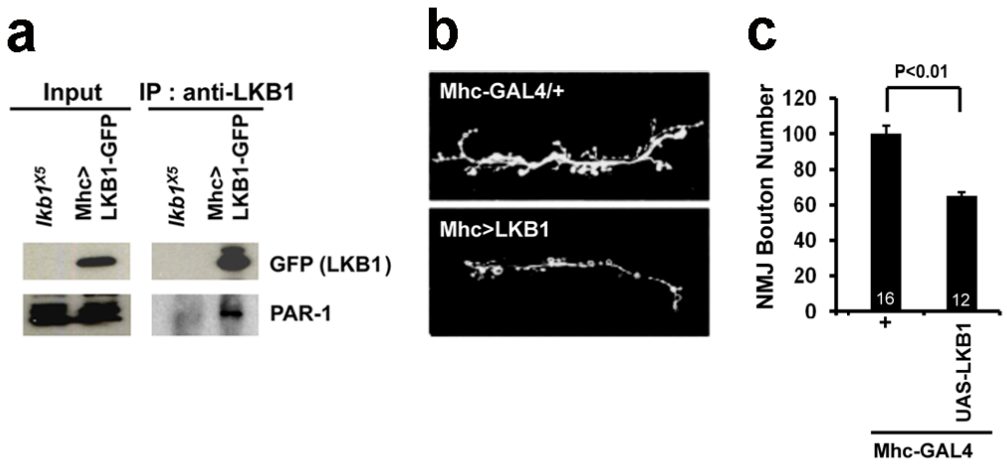

Supplementary Figure S15. I*n vivo* physical interaction between LKB1 and PAR-1 and effects of LKB1 GOF on synaptic morphology. (a) PAR-1 physically interacts with LKB1. Larval body-wall muscle extracts from *Mhc-Gal4>UAS-LKB1-GFP* or $lkb1^{X5}$ null mutant animals were immunoprecipitated with anti-LKB1, and the presence of endogenous PAR-1 in the IP complex was detected by western blot analysis with an anti-PAR-1 antibody. **(b)** Representative immunostaining showing larval NMJ morphology in animals overexpressing LKB1 pre- or post-synaptically. **(c)** Quantification of data shown in B. The total number of boutons per muscle area on muscle 6/7 of A3 is measured. N indicates the number of animals analyzed. The error bars represent means ± SEM. *P*-values were determined using two-tailed Student's *t*-test for each comparison. Experiments were performed in triplicate.

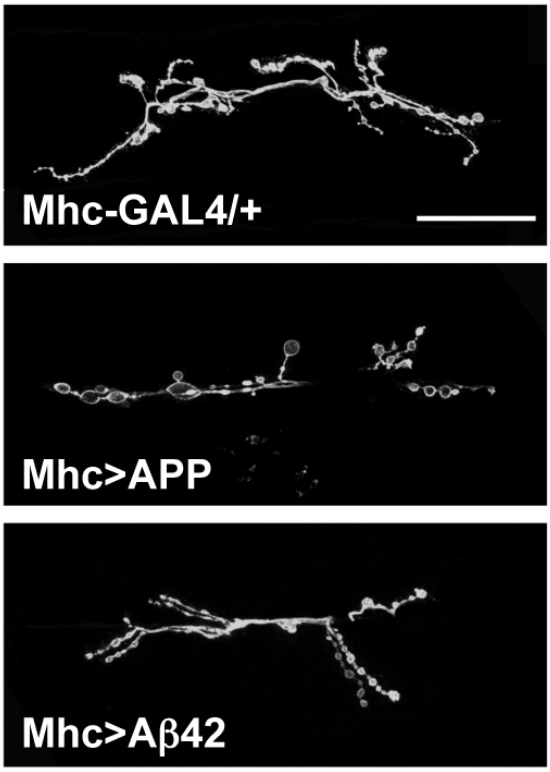

Supplementary Figure S16. Postsynaptic overexpression of APP or Aβ42 leads to a decrease in NMJ bouton number. Representative HRP immunostainings showing larval NMJ morphology of the indicated genotypes are shown. *Mhc-GAL4/+* and *Mhc-Gal4>UAS-APP* were grown at 29^{o}C and *Mhc-Gal4>UAS-Aβ42* at 25^{o}C. Scale bar, 50 μm.

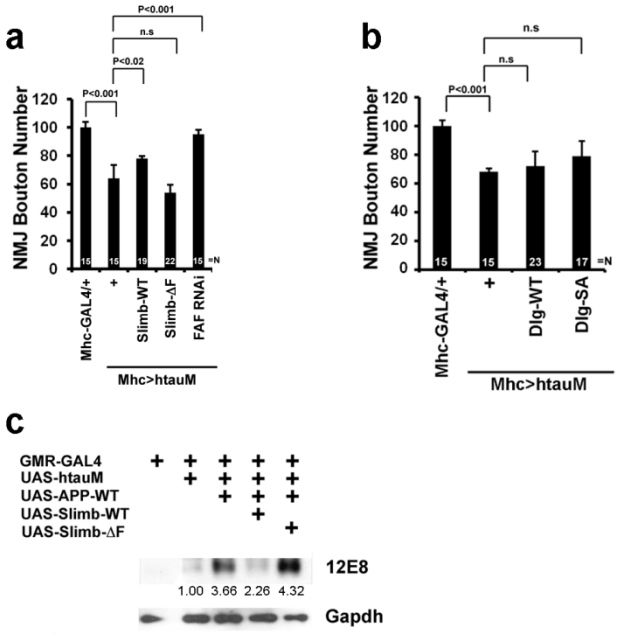

Supplementary Figure S17. Genetic interactions between tau and Slimb/FAF or between tau and Dlg, and the effects of APP and Slimb interaction on tau phosphorylation at 12E8 sites. (a) Quantification of larval NMJ bouton number showing genetic interaction between htauM and Slimb or FAF. The synapse loss phenotype seen in *Mhc-Gal4>UAS-htauM* background was partially rescued by the co-expression of Slimb-WT or FAF RNAi. N indicates the number of animals analyzed. The error bars represent means ± SEM. *P*-values were determined using two-tailed Student's *t*-test for each comparison. Experiments were performed in triplicate. **(b)** Quantification of NMJ bouton number testing possible genetic interaction between htauM and Dlg variants at the NMJ. N indicates the number of animals analyzed. No interaction was detected. N indicates the number of animals analyzed. The error bars represent means ± SEM. *P*-values were determined using two-tailed Student's *t*-test for each comparison. Experiments were performed in triplicate. **(c)** Western blot analysis of 12E8-positive p-htau level after co-expression of Slimb-WT or Slimb-ΔF in *GMR-Gal4>UAS-htauM+UAS-APP-WT* background. Gapdh serves as a loading control. Values represent 12E8-positive p-tau level in the indicated genotypes normalized with *GMR-Gal4>UAS-htauM* control in three independent experiments.